Assessment of the sound reduction index of building elements by near field excitation through an array of loudspeakers and structural response measurements by laser Doppler vibrometry

N.B. Roozen, Quentin Leclere, D. Urbán, L. Kritly, C. Glorieux

Assessment of the sound reduction index of building elements by near field excitation through an array of loudspeakers and structural response measurements by laser Doppler vibrometry

N.B. Roozen[1)*], Q. Leclère[2)], D. Urbán[3)], L. Kritly[1)], C. Glorieux[1)]
[1)] KU Leuven ,Laboratory Acoustics, Soft Matter and Biophysics,
Department of Physics and Astronomy, KU Leuven, Celestijnenlaan 200D, B3001 Heverlee, Belgium.
[2)] Univ Lyon, INSA-Lyon, LVA EA677, F-69621 Villeurbanne, France.
[3)] Slovak University of Technology in Bratislava, Faculty of Civil Engineering,
Radlinského 11, 810 05 Bratislava, Slovakia.

Summary

At low frequencies the assessment of the sound reduction index of building elements in the laboratory according to the standard ISO 10140-2:2010 is burdened by a large variation in the measurement results. This is due to the fact that at low frequencies the acoustic field is not sufficiently diffuse.

This paper discusses a measurement procedure in which a diffuse field is created in the source room by means of an array of loudspeakers positioned closely to the building insulation element under test. This procedure exploits the acoustic near field of the loudspeaker array.

The problems related to the breakdown of the diffuse field assumption of the receiving room are eliminated by measuring the structural response of the building insulation element under test by means of laser Doppler vibrometry and the application of the Rayleigh integral to compute the radiated sound power. The sound reduction index is determined from the ratio of the incident sound power, created by the loudspeaker array, and the radiated sound power.

The measurement approach is validated by means of a measurement of the sound reduction index of a single layer glazing. Comparisons are made with an analytical model and with a standardized ISO 10140-2:2010 measurement. Although the method offers clear, strong points in terms of removing room acoustic effects from the measurements in the lower frequency range, a point of concern is the measurement effort.

1 Introduction

Insufficient low-frequency sound insulation between dwellings combined with the use of powerful music reproduction systems is one aspect why inhabitants are often disturbed by their neighbors. Over the last years, an increased interest in sound insulation at low frequencies can be observed. Although in current standards the assessment of sound insulation in the frequency range down to 50Hz is still optional [1, 2], most studies recommend the inclusion of frequencies below 100 Hz [3, 4]. However, it is also well known that measurents of the sound reduction index according to the standard ISO 10140:2010 [5] at frequencies below 100 Hz are affected by a large uncertainty [6, 7, 8]. The reason for this uncertainty is the reduced modal density of the acoustic eigenmodes at lower frequencies, in both the source room and the receiving room of the test facility. The resulting modal behavior cause the acoustic field to deviate from the ideal diffuse field [9, 10, 11]. This makes the measurement results obtained in a specific testing laboratory strongly dependent on the chosen microphone positions and therefore uncertain. Moreover, as the obtained measurement result is dependent on the specific geometry of the transmission suite, it also causes a poor reproducibility between laboratories [12, 13].

In the works of Bravo, Maury and Elliott [12, 14] the breakdown of the diffuse field assumption of the source room was reduced by using a number of suitably driven loudspeakers close to the building insulation element under test to create a diffuse incident field as closely as possible. To assess the acoustic power transmitted through the element under test, they measured the acoustic sound intensity at a dense array of points at the receiving side, close to the element. However, the effect of the receiving room was found not to be reduced in this way. The influence of the receiving room on the transmitted power, using the sound intensity approach, can only be reduced by the use of moving diffusers in the receiving room, or if a larger and more anechoic receiving room is used [12].

*corresponding author, currently working at A&Z Acoustics, Bratislava, bert.roozen@euroakustik.sk

Roozen et al. [15] showed that the sound power radiated by a building insulation element under test at low frequencies can be determined from the vibration pattern of the building element, using laser Doppler vibrometry (LDV) or other vibration measurement techniques. The radiated sound power was calculated from the measurement data by means of the Rayleigh integral, in which an infinite half space is assumed for the 'receiving room'. In this manner the computed sound power is not affected by the room acoustic modes of the receiving room.

In the present paper the works of Bravo et al. [14] and Roozen et al. [15] are combined. The diffuse excitation field is created by a loudspeaker array closely positioned to the building element under test, and the radiated sound power is determined by means of laser Doppler vibrometry.

The paper is organized as follows. Section 2 treats the synthesis of the diffuse sound field by means of a loudspeaker array. This section also discusses the computation of the radiated sound power level, using conditioned spectral analysis. Section 3 reports about measurements on a single glazing, and validates the results by means of an analytical model. A comparison with a standardized ISO 10140:2010 [5] measurement is given as well. Section 4 draws the conclusions of the work.

2 Theory for the synthesis of a diffuse field and the analysis of the measurement data

The theory to synthesize spatially correlated random pressure fields is well documented in literature [16]. In this section it is briefly summarized for the sake of completeness. In addition to this brief summary, a proposal is elaborated to perform the analysis of the measurement data by means of a conditioned spectral analysis, which is different from the approach taken by Elliott, Bravo and Maury et al. [14, 16, 17, 18].

2.1 The synthesis of spatially correlated random pressure fields

Piersol [19] showed that the cross spectral density of the sound pressure of a diffuse acoustic field, measured between two points separated at a distance r from each other, is given by (see also [20, 21, 22, 23])

$$S_D \frac{sin(kr)}{kr} \tag{1}$$

where $k = \omega/c$ is the acoustic wavenumber, ω is the angular frequency ($\omega = 2\pi f$) and S_D is the autopower spectrum level of the desired diffuse acoustic field. S_D is a frequency dependent scalar, independent of the position in the room.

Let the matrix with desired cross spectral densities at the N_{mic} control microphone positions, based on Eq. 1, be denoted by $\mathbf{S_{dd}}$. The subscript $_\mathbf{d}$ indicates the desired diffuse field. The control microphones are positioned on the surface of the building element in a rectangular grid, between the loudspeaker array and the building element. The matrix $\mathbf{S_{dd}}$ has a dimension $N_{mic} \times N_{mic}$ for each frequency being considered, and the rank of this matrix is equal to N_{mic}.

To approximate the acoustic field with the above mentioned cross spectral density as closely as possible a discrete number of loudspeakers, N_{LS}, is used. The number of control microphone positions, N_{mic}, is normally larger than the number of loudspeakers, N_{LS}. However, having N_{LS} signals available to create the desired acoustic field, that field cannot have a rank higher than N_{LS}. Therefore, a limited number of uncorrelated principal components of the desired acoustic field are considered, following Elliott et al. [16]. For this purpose the matrix $\mathbf{S_{dd}}$ is decomposed in its eigenvectors $\mathbf{V}$ and its eigenvalues $\mathbf{\Lambda}$:

$$\mathbf{S_{dd}} = \mathbf{V}\mathbf{\Lambda}\mathbf{V}^* \tag{2}$$

where * denotes the complex conjugate.

The best least-squares approximation to $\mathbf{S_{dd}}$ with rank N_{LS} can be obtained by taking the N_{LS} terms with the largest eigenvalues:

$$\tilde{\mathbf{S}}_{\mathbf{dd}} = \tilde{\mathbf{V}}\tilde{\mathbf{\Lambda}}\tilde{\mathbf{V}}^* \tag{3}$$

where $\tilde{\mathbf{\Lambda}}$ is a diagonal matrix that contains the N_{LS} largest eigenvalues, and the matrix $\tilde{\mathbf{V}}$ contains the N_{LS} largest eigenvectors. The tilde $\tilde{}$ indicates that the variable is the best least-squares approximation with rank N_{LS}. In the approximation of interest, the rank of matrix $\tilde{\mathbf{S}}_{\mathbf{dd}}$ is forced to be equal to the number of loudspeakers of the loudspeaker array, N_{LS}, being the maximal feasible rank the can be created by the array.

The N_{LS} input signals to the loudspeaker amplifiers required to generate the desired cross spectral matrix $\tilde{\mathbf{S}}_{\mathbf{dd}}$ at the control microphones can be constructed as follows. A measurement is performed to relate the N_{LS} input signals $\mathbf{x}$ to the pressures $\mathbf{y}$ as measured at the N_{mic} control microphone positions (for a system diagram, see Fig. 1). This results in a relationship in the frequency domain that reads

$$\mathbf{Y} = \mathbf{H}\mathbf{X} \tag{4}$$

where $\mathbf{H}$ is a matrix of transfer functions having a dimension $N_{mic} \times N_{LS}$ for each frequency being considered, vector $\mathbf{Y}$ is the Fourier transform of the control microphone signals, having a dimension $N_{mic} \times 1$, for each frequency being considered, and vector $\mathbf{X}$ is the Fourier transform of the input signals to the loudspeaker amplifiers, having a dimension $N_{LS} \times 1$ for each frequency being considered. The matrix with optimal control filters $\mathbf{W}_{opt}$ can be computed from

$$\mathbf{W}_{opt} = (\mathbf{H}^*\mathbf{H})^{-1}\mathbf{H}^*\tilde{\mathbf{U}}\tilde{\mathbf{\Lambda}}^{1/2} \tag{5}$$

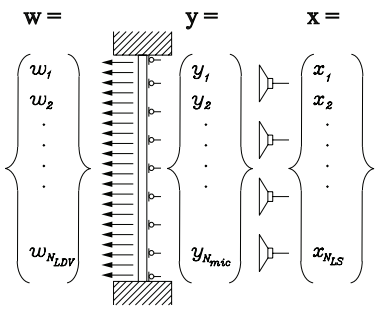

Figure 1: System diagram with input signals to the loudspeaker amplifiers $\mathbf{x}$, microphone control signals $\mathbf{y}$, and response of the building insulation element under test $\mathbf{w}$.

where $\tilde{\mathbf{U}}$ represents N_{LS} uncorrelated random signals with unitary variances in the frequency domain. Using this matrix with optimal control filters, the optimal input signals to the loudspeaker amplifiers $\mathbf{X}$ can be computed with

$$\mathbf{X} = \mathbf{W}_{opt}\tilde{\mathbf{U}} \tag{6}$$

The time domain signals $\mathbf{x}$ to drive the loudspeaker array can be obtained from the matrix $\mathbf{X}$ by means of an inverse Fourier transform. For a more extensive description of the synthesis of a diffuse field by means of a loudspeaker array, see Elliott et al. [16].

2.2 Analysis of measurement data by means of conditioned spectral analysis, CSA

Using the optimal loudspeaker signals $\mathbf{x}$, a diffuse acoustic field with cross spectral matrix $\tilde{\mathbf{S}}_{\mathbf{dd}}$ is obtained. As this excitation field consists of N_{LS} uncorrelated principal components, as discussed in the previous section, also the structural response $\mathbf{w}$ of the building insulation element under test will consists of the same number of principal components. These N_{LS} uncorrelated response components are denoted by $\mathbf{w}^{(k)}$, with $k = 1...N_{LS}$.

The uncorrelated response components can be extracted by means of Conditioned Spectral Analysis (CSA, after Bendat and Piersol [24]) or by means of virtual source analysis (VSA, after Price and Bernhard [25]). The advantage of both approaches is that the radiated sound powers that follow from these uncorrelated responses can be simply added to obtain the total radiated sound power, as explained by Leclere [26]. In this paper, the CSA approach was taken, which will be outlined briefly below.

Having measured the cross spectra between the response signals $\mathbf{w}$ and reference signals $\mathbf{x}$, $\mathbf{S}_{\mathbf{wx}}$, and the auto spectra of the reference signals, $\mathbf{S}_{\mathbf{xx}}$, the first uncorrelated contributions $\mathbf{w}^{(1)}$ can be computed from

$$w_i^{(1)} = S_{w_i x_1}/\sqrt{S_{x_1 x_1}}, \qquad i = 1...N_{LDV} \tag{7}$$

where $S_{w_i x_j}$ is the (i,j)-th component of the matrix $\mathbf{S}_{\mathbf{wx}}$, $S_{x_j x_j}$ is the (j,j)-th component of the matrix $\mathbf{S}_{\mathbf{xx}}$, and $w_i^{(1)}$ is the i-th component of the vector $\mathbf{w}^{(1)}$. In this notation the indexes range as $i = 1...N_{LDV}$ and $j = 1...N_{LS}$.

The second uncorrelated contributions $\mathbf{w}^{(2)}$ can be computed by removing the energy in the spectral matrices which is coherent with the first reference:

$$S^{(1)_{rem}}_{w_i x_j} = S_{w_i x_j} - \frac{S_{w_i x_1} S_{x_1 x_j}}{S_{x_1 x_1}}, \quad \begin{matrix} i = 1...N_{LDV}, \\ j = 1...N_{LS} \end{matrix} \tag{8}$$

and

$$S^{(1)_{rem}}_{x_j x_j} = S_{x_j x_j} - \frac{|S_{x_j x_1}|^2}{S_{x_1 x_1}}, \quad j = 1...N_{LS} \tag{9}$$

Using these conditioned auto and cross spectra the second uncorrelated contributions, $\mathbf{w}^{(2)}$ can be computed as follows

$$w_i^{(2)} = S^{(1)_{rem}}_{w_i x_2}/\sqrt{S^{(1)_{rem}}_{x_2 x_2}}, \qquad i = 1...N_{LDV} \tag{10}$$

The k-th uncorrelated contributions $\mathbf{w}^{(k)}$ can be computed from

$$w_i^{(k)} = S^{(k-1)_{rem}}_{w_i x_k}/\sqrt{S^{(k-1)_{rem}}_{x_k x_k}}, \quad \begin{matrix} i = 1...N_{LDV}, \\ k = 2...N_{LS} \end{matrix} \tag{11}$$

where the conditioned auto and cross spectra are computed from the previously computed conditioned spectra:

$$S^{(k)_{rem}}_{w_i x_j} = S^{(k-1)_{rem}}_{w_i x_j} - \frac{S^{(k-1)_{rem}}_{w_i x_k} S^{(k-1)_{rem}}_{x_k x_j}}{S^{(k-1)_{rem}}_{x_k x_k}}, \quad \begin{matrix} i = 1...N_{LDV}, \\ j = 1...N_{LS}, \\ k = 2...N_{LS} \end{matrix} \tag{12}$$

and

$$S^{(k)_{rem}}_{x_j x_j} = S^{(k-1)_{rem}}_{x_j x_j} - \frac{|S^{(k-1)_{rem}}_{x_j x_k}|^2}{S^{(k-1)_{rem}}_{x_k x_k}}, \quad \begin{matrix} j = 1...N_{LS}, \\ k = 2...N_{LS} \end{matrix} \tag{13}$$

The multiple coherence [24] can be defined by the ratio of the energy contained in the sum of the uncorrelated contributions $\mathbf{w}^{(k)}$ to the total energy contained in $\mathbf{w}$:

$$\gamma_i = \frac{\sum_{k=1}^{N_{LS}} |w_i^{(k)}|^2}{S_{w_i w_i}} \qquad i = 1...N_{LDV} \tag{14}$$

Having computed all N_{LS} uncorrelated contributions $\mathbf{w}^{(k)}$, $k = 1...N_{LS}$, the sound power radiated by each of the uncorrelated responses, $\Pi^{(k)}_{rad}$, can be determined. In this work the radiated sound power is computed by means of the Rayleigh integral, following [15]. Using this approach the building insulation element under test is assumed to be baffled, and the receiving acoustic domain is a semi-infinite acoustic domain. In this manner the room acoustic effects of the receiving room are eliminated. In Appendix A the numerical procedure is briefly outlined.

As $\mathbf{w}^{(k)}$, $k = 1...N_{LS}$, contain the uncorrelated responses of the building element under test, extracted by CSA, the sound power radiated by each of the responses $\mathbf{w}^{(k)}$ are also uncorrelated to each other. Because of this property, the total sound power radiated by the building element can be computed as the sum of the sound power components $\Pi_{rad}^{(k)}$:

$$\Pi_{rad} = \sum_{k=1}^{N_{LS}} \Pi_{rad}^{(k)} \tag{15}$$

Note that it is essential to compute the (complex valued) uncorrelated responses $\mathbf{w}^{(k)}$, $k = 1...N_{LS}$, to allow a correct computation of the radiated powers of each of the uncorrelated responses. The phase information contained in each of the uncorrelated responses $\mathbf{w}^{(k)}$ is an essential aspect in the computation of the radiated power $\Pi_{rad}^{(k)}$ by means of the Rayleigh integral.

In literature it is mentioned that the accuracy of the results of the CSA approach in source identification problems strongly depends upon the elimination order of the references [27, 28]. However, the context of the present work is not related to the separation of source contributions, it is just needed here to separate uncorrelated responses referenced to a set of arbitrary inputs. In such a case the total sound power level Π_{rad} is not affected by the ordering of references.

Whilst driving the loudspeaker array with the optimal loudspeaker signals, $\mathbf{x}$, the sound pressure levels at the grid of control points (N_{mic} points) need to be measured. From the blocked pressure squared, spatially averaged over the N_{mic} control points, $\overline{p_{bl}^2}$, the incident sound power can be estimated by

$$\Pi_{inc} = \frac{S}{4\rho c}\frac{1}{2}\overline{p_{bl}^2} = \frac{S}{8\rho c}\overline{p_{bl}^2} \tag{16}$$

where S is the surface area of the building insulation element under test and where the factor $1/2$ arises from the reflections on the rigid wall [29, 30]. The blocked pressure p_{bl} is the pressure acting on the building insulation element under test, where it is assumed that the impedance of the building element under test is infinitely large (in analogy with the term 'blocked force' as introduced by Gardonio and Brennan [31]).

Finally, from the incident and radiated sound powers, the sound reduction index R of the building insulation element under test can be estimated:

$$R = \frac{\Pi_{inc}}{\Pi_{rad}} \tag{17}$$

To summarize, the following data needs to be measured:

- The matrix of transfer functions $\mathbf{H}$ between the acoustic responses $\mathbf{y}$ and the loudspeaker signals $\mathbf{x}$ with dimension $N_{mic} \times N_{LS}$,
- The cross spectra of the structural responses $\mathbf{w}$ and the loudspeaker signals $\mathbf{x}$ with dimension $N_{LDV} \times N_{LS}$, whilst driving the loudspeaker array with the optimal signals $\mathbf{x}$, extracted from analysis of the signals obtained in step 1,
- The cross spectra of the acoustic responses $\mathbf{y}$ and the loudspeaker signals $\mathbf{x}$, with dimension $N_{mic} \times N_{LS}$, whilst driving the loudspeaker array with the optimal signals $\mathbf{x}$, to allow the computation of the incident power.

3 Measurements

Two types of measurements were performed: measurements according to the ISO 10140-2:2010 standard [5], and measurements by means of the loudspeaker array placed close to the device under test, of which the theory was described in the previous section. Section 3.1 discusses the measurement set-up and Section 3.2 the results.

3.1 Measurement set-up

The measurements were performed on a single glazing with a lateral dimension of 1.35 × 1.54 m^2 and a thickness of 12 mm. The mass per unit area was measured to be 28.8 kg/m^2. The glazing was mounted in a test opening of 1.37 × 1.555 m^2, covered by a wooden frame and sealed by putty. The dimensions of the source and the receiving room are approximately 4.11 m (height) × 5.10 m × 4.14 m, which yields a volume of 87 m^3 each.

The text below details the set-up for the measurements by means of an array of loudspeakers and a scanning laser Doppler vibrometer.

An array of N_{LS}=12 loudspeakers in an arrangement of 3×4 was constructed (see Fig. 3). Each loudspeaker, a 12inch woofer type Visaton W300-8, was mounted in it's own cabinet made from 18mm plywood to prevent acoustic cross-talk with neighboring speakers. The loudspeaker array cabinet, with a total lateral dimension of 1.25 × 1.50 m^2, was put at a distance of 20 cm from the glazing, which corresponds to about half the distance between two adjacent loudspeakers. This distance is a bit closer but still of the same order of magnitude as was done in the work of Bravo [17].

With this loudspeaker array, an acoustic field can be controlled having a minimum acoustic wavelength twice the inter distance of the loudspeakers, following the sampling theorem of Shannon [32]. With an inter distance of 0.41 m and 0.37 m in horizontal and vertical direction, respectively, this corresponds to a theoretical maximum frequency of 415 Hz and 450 Hz, respectively, taking the speed of sound c=340 m/s.

The matrix of transfer functions $\mathbf{H}$ of dimension $N_{mic} \times N_{LS}$ for each frequency considered was mea-

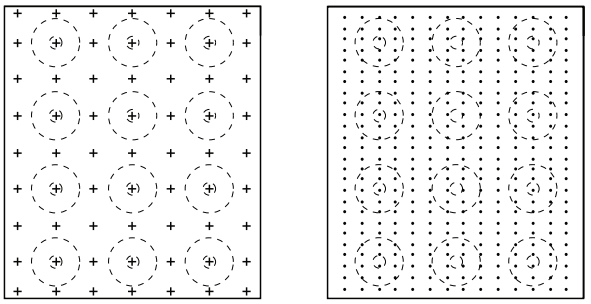

(a) Control microphone grid (7 × 9, indicated by crosses)

(b) Laser Doppler velocimetry grid (14 × 19, indicated by dots)

Figure 2: Measurement grids on the glazing, LS-array indicated by dashed lines.

sured by driving each loudspeaker individually and measuring the acoustic response at N_{mic}=7 × 9=63 positions, sequentially in time. The measurement grid is indicated in Fig. 2a. With this matrix, the optimal loudspeaker signals $\mathbf{x}$ were computed off-line, as detailed in Section 2.1.

The control microphone grid was chosen twice as fine as compared to the loudspeaker grid in order to have enough redundancy to construct the optimal signals to drive the loudspeaker array. The maximum frequency that can be controlled by the loudspeaker array, however, is determined by the inter spacing of the loudspeakers (with a theoretical value of 415 Hz as estimated above).

Next, the glass plate was excited by the loudspeaker array using the optimal loudspeaker signals $\mathbf{x}$, measuring the response of the glazing $\mathbf{w}$ by means of an in-house developed scanning laser Doppler measurement system, consisting of a Polytec laser head OFV-505, a Polytec controller OFV-5000, and a dual-axis scanning mirror system from Thorlabs (see Fig. 5). A measurement grid of N_{LDV}=14 × 19=266 positions was chosen (see Fig. 2b). On the glazing retro-reflecting stickers were glued (see Fig. 4) to increase the optical reflection, facilitating the laser Doppler measurement.

Using Kirchhoff's thin shell theory of an infinite plate, an approximate estimate of the structural wavelength of the glazing of about 0.5 m was obtained at the maximum frequency that can be controlled by the loudspeaker array (415 Hz). According to the sampling theorem of Shannon [32] this would require a mesh of 2·1.35/0.5=5 × 2·1.54/0.5=6 points. Taking 6 points per wavelength, a mesh of 6·1.35/0.5=16 × 6·1.54/0.5=19 would be required. A mesh of 14 × 19 was chosen.

The loudspeakers were driven by a set of amplifiers, 12 in total, and two inter-connected Roland data acquisition systems, type Octa Capture (8 input channels, 8 output) and type Studio Capture (16 input channels, 8 output) (see Fig. 6). With the inter-connected Roland data acquisition systems the

Figure 3: LS-array in front of glass plate.

Figure 4: Glazing with retro-reflecting stickers at one side, a microphone mounted on the other side of the glass plate (traversed from one position to the other), and the loudspeaker array also on the other side of the glass plate.

structural response as well as the acoustic response were measured, including the signals that were used to drive the loudspeakers (via a loop back).

3.2 Measurement results

3.2.1 Estimation of the sound reduction index according to the standard

The sound reduction index of the glazing was measured according to the ISO 10140-2:2010 standard [5]. During this measurement the loudspeaker array was not in the source room. Instead, two loudspeakers, brand name Mackie, type SRM450 were positioned in the corners of the source room, opposite of the test opening, to excite the glazing. In our experience, these loudspeakers are capable to generate noise from the 31.5 Hz $1/3^{rd}$ octave band onwards, as well as (but with reduced level) in the 25 Hz $1/3^{rd}$ octave band. The sound pressure level in the source room L_{p1} was averaged over 8 microphone positions. The reverberation time T_{60} and the sound pressure level in the receiving room L_{p2} were also averaged over 8 microphone positions. From these measurement data the sound reduction index R of the glazing was com-

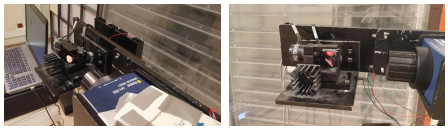

Figure 5: The in-house developed scanning Laser Doppler vibrometry measurement system.

Figure 6: Power amplifiers (left) and data acquisition measurement systems (right).

puted with the equation

$$R = L_{p1} - L_{p2} + 10 \lg \left(\frac{S}{A} \right) \tag{18}$$

where S is the area of the free test opening in which the element is mounted, and A the equivalent sound absorption area in the receiving room, which is related to T_{60} according to Sabine's formula as $T_{60} = 0.16V/A$, where V is the volume of the receiving room.

Figure 7 shows the measured sound reduction index. The figure also shows the coincidence frequency, which is estimated to be approximately 1000 Hz (12 mm thick glass plate, Young's modulus 56 GPa, density 2400 kg/m^3). Indeed, around the coincidence frequency the sound reduction index R shows a brad dip, as expected. Although the ISO 10140-2:2010 standard prescribes to use 1/3$^{\text{rd}}$ octave bands from 50 Hz onwards, also frequency bands below 50 Hz are shown. To slightly improve the accuracy of the measurements in the low frequency range, the number of microphone positions was increased from the required 5 (ISO 10140) to 8 positions.

The uncertainty in the measured sound reduction index can be determined by considering the standard deviation of the sound pressure levels in the source and receiving room from position to position, $\sigma_{L_{p1}}$ and $\sigma_{L_{p2}}$, respectively, as well as the standard deviation of the equivalent sound absorption in the receiving room resulting from the reverberation time standard deviation [33]. Given that the contributions of the individual terms to the total uncertainty on R are independent, the combined uncertainty can then be estimated as $\sigma_R = \sqrt{\sigma^2_{L_{p1}} + \sigma^2_{L_{p2}} + \sigma^2_{10 \lg(A)}}$. In case of repeated measurements on N (eight) positions, it can be expected that the error on the mean reduces to $\sigma_{R,\overline{x}} = \sigma_R/\sqrt{N}$. In addition to the ISO-based results, Figure 7 also shows the measured sound reduction index incremented and decremented with its standard deviation σ_R and standard error $\sigma_{R,\overline{x}}$.

3.2.2 Estimation of the sound reduction index by means of an array of loudspeakers and laser Doppler vibrometry

The sound reduction index of the glazing was measured by exciting the glazing by means of a diffuse sound field created by a near field array of loudspeakers and measuring the glass panel response by means of laser Doppler vibrometry.

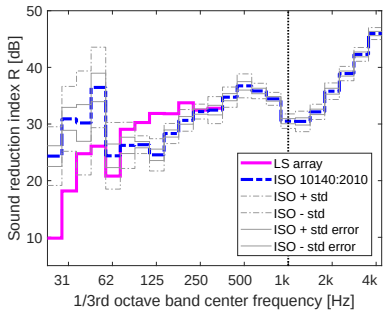

Figure 7: Sound reduction index measurement results according to the ISO 10140-2:2010 standard, including frequencies below 50 Hz (mean value as a thick dashed blue curve, mean value incremented and decremented with the standard deviation as thin dashed blue curves), compared with sound reduction index 1/3$^{\text{rd}}$ octave results obtained by means of an array of loudspeakers and a scanning laser Doppler (solid magenta curve). The interval between the dash-dotted and full gray lines indicate the estimated standard deviation between measurements on different microphone positions and the standard error on their mean respectively. The coincidence frequency of the glass plate (approximately 1000 Hz) is indicated by a vertical dashed line.

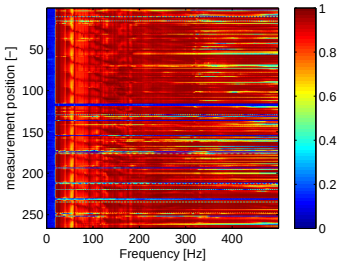

(a) Laser Doppler data

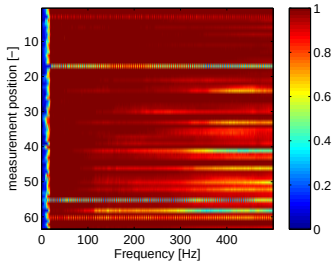

(b) Microphone data

Figure 8: Multiple coherence between the response data and the reference signals, based on CSA.

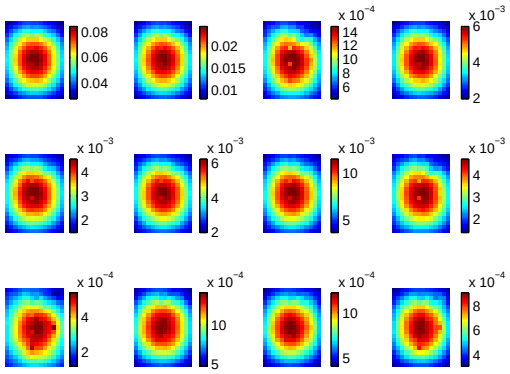

(a) 27.5 Hz

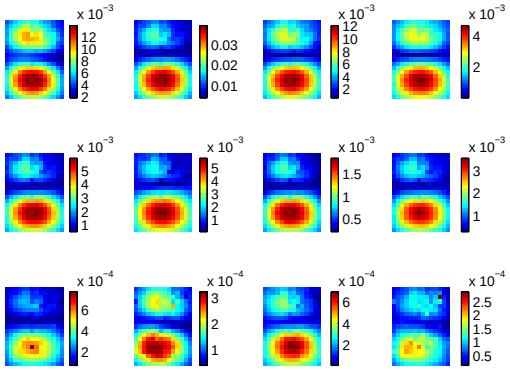

(b) 61.75 Hz

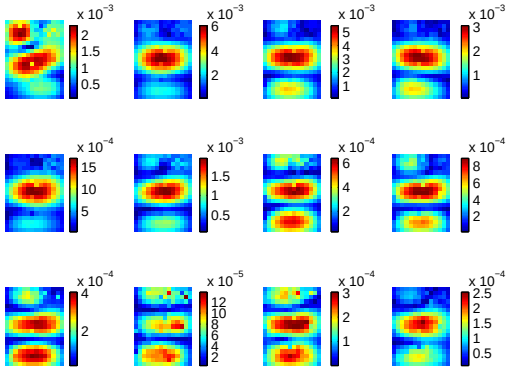

(c) 118 Hz

Figure 9: Largest 12 principal components of the Rayleigh computed sound pressure distribution on the glass plate (units: Pa, spectral amplitude, frequency resolution: 0.1 Hz), computed by CSA.

Driving the loudspeaker array by means of the optimal loudspeaker signals $\mathbf{x}$, the structural responses $\mathbf{w}$ of the building insulation element under test and the acoustic pressure responses $\mathbf{y}$ close to the building insulation element under test were measured. In [34] it was shown that the measurement record length needs to be larger than the reverberation time of the structural-acoustic system to avoid serious errors in the frequency response function estimate. As the reverberation time of the source room is about 3 seconds, a measurement record length of 10 seconds was chosen, yielding a spectral resolution of 0.1 Hz. A Hanning weighting function was applied. The number of averages was 20, with 75% overlap, requiring a total measurement time of 60 seconds per point. The multiple coherence (as defined in Eqn. 14) of the structural and acoustic measurements is shown in Fig. 8.

The multiple coherence of laser Doppler velocimetry measurements (Fig. 8a) overall shows a good coherence, close to unity, except for a few measurement points (e.g. measurement points 116-118), which was caused by a bad optical reflection of the laser beam at those points. The Multiple coherence of the microphone measurement close to the glass panel (in the source room, see Fig 8b) shows coherences close to unity as well, except for a few measurement points. Below 20 Hz the multiple coherence of laser Doppler velocimetry and the acoustic measurement drops steeply due to the fact that the signal sent to the loudspeaker array did not contain energy at frequencies below 20 Hz.

The multiple coherences shown in Fig. 8 were obtained after correcting for latencies between the two inter-connected Roland data acquisition systems. An adequate clock-synchronization appeared not to be feasible. The latency correction was possible as the loudspeaker driving signals were looped back to both Roland data acquisition systems. Without latency correction the multiple coherence is significantly lower, varying between 0.1 and 0.9 at random, for all frequencies considered.

Figure 9 shows the Rayleigh computed sound pressure amplitudes based on the 12 principal components of the glazing response, using CSA. Three frequencies were chosen to illustrate the vibrational behavior at resonant frequencies of the glazing. The fundamental frequency occurs at 28 Hz. The second mode occurs at 62 Hz and a third mode occurs at 118 Hz.

Figure 10 shows the Rayleigh computed active sound power radiated by the glazing, using Eq. 15. The total sound power clearly shows peaks at the above mentioned resonance frequencies of 28 Hz, 62 Hz and 118 Hz.

Figure 11 shows the total radiated sound power as in the previous figure, as well as the incident acoustic power calculated by means of Eq. 16. The incident acoustic power generated by the loudspeaker array

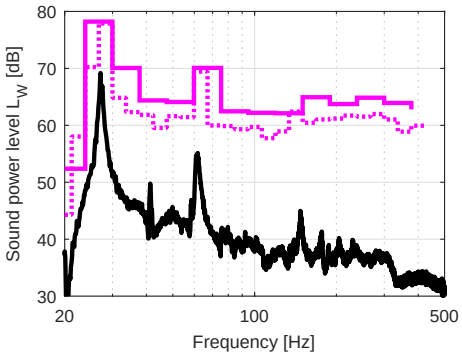

Figure 10: Radiated active sound power, computed from Eq. 15. The bold black curve shows the narrow band spectrum of the total sound power, computed as the sum of the individual CSA powers. The bold magenta curve shows the $1/3^{\text{rd}}$ octave spectrum. The dashed magenta curve shows the $1/12^{th}$ octave spectrum.

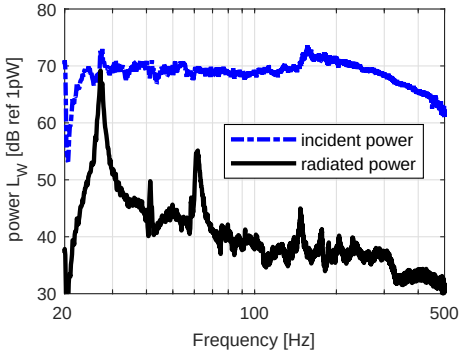

Figure 11: Narrowband incident sound power spectrum (dashed blue curve) and radiated sound power spectrum (solid black curve), glass panel excited by 12 LS array close to the glass panel, frequency resolution: 0.1 Hz, computed by means of CSA according to Eq. 16 and Eq. 15, respectively.

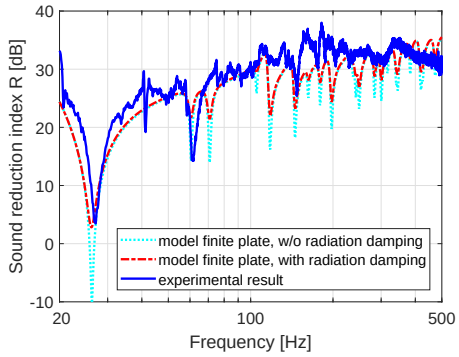

Figure 12: Narrowband sound reduction index R obtained by means of the LS array and laser Doppler vibrometry of the glazing (blue solid curve), compared with the analytically obtained sound reduction index R of a simply-supported plate, with (red dashed curve) and without(magenta dotted curve) taking into account radiation damping.

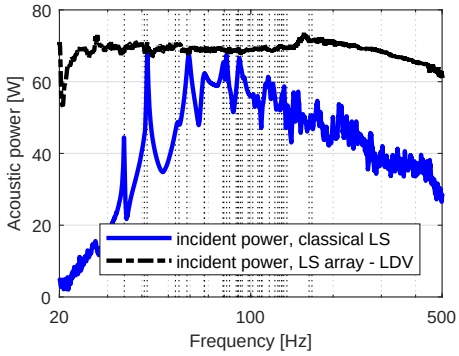

(a)

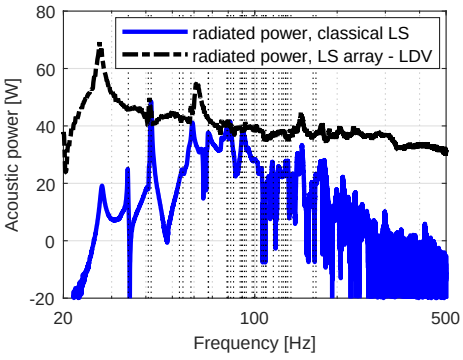

(b)

Figure 13: Narrowband sound power spectrum obtained with loudspeakers in the corners of the sending room (solid blue curves) and obtained with the loudspeaker array close to the device under test (dashed black curves), a) incident sound power spectrum computed from Eq. 16, b) radiated sound power spectrum computed from Eq. 15. The acoustic resonance frequencies of the source room up to 160 Hz are indicated by vertical dotted black lines.

has a reasonably flat frequency spectrum, indicating that the room resonances of the source room was effectively suppressed.

Taking the ratio between the incident power to the radiated power (Eq. 17) gives the sound reduction index, as shown in Fig. 12 in terms of narrow frequency bands and in Fig. 7 in terms of $1/3^{\text{rd}}$-octave frequency bands.

In Fig. 12 the obtained results are compared with a theoretical estimate of the sound reduction index. This estimate is based upon an analytical expression of the structural-dynamics of a simply supported plate, having dimension L_x=1.35 m, L_y=1.54 m, thickness h=12e-3 m, Young's modulus E=56 GPa, Poisson's ratio ν=0.24, density ρ=2400 kg/m^3 and loss factor η=0.013.

The density ρ of the glass was extracted from a weight measurement of the glass panel, and the measurement of its dimensions. The Young's modulus E was tuned in order to get a reasonable agreement between the first resonance frequency as predicted by the analytical model and the experimentally obtained first resonance frequency. The loss factor η was extracted from the half power (-3 dB) bandwidth of the measured transfer function at the first resonance frequency of the glazing. It should be noted that the damping as specified in the analytical model is valid at the first resonance frequency only. Thus, the analytical model has a limited frequency range in which it is accurate.

From the mobility of the simply-supported plate (for which theoretical expressions are readily available), an estimate of the sound reduction index R for a diffuse sound field excitation is computed (see [35] for details about this approach). Figure 12 shows the results for two cases: with and without taking into account the radiation damping of the plate. The results with the radiation damping taken into account correspond reasonably well with the R obtained by means of an array of loudspeakers and laser Doppler vibrometry, which validates the latter approach. Deviations up to 5 dB are observed, which are likely to be caused by the limited accuracy of the analytical model to represent the device under test.

To illustrate the effectiveness of the loudspeaker array to suppress room modes in the source room, an additional measurement was performed with classical loudspeakers in the corners of the source room. The loudspeaker array was removed from the room for this experiment. The blocking sound pressure levels at the surface of the glazing and the response of the glazing were measured, from which the incident and the radiated sound powers were computed with Eq. 16 and Eq. 15, respectively. The results are shown in Fig. 13, in which the acoustic resonance frequencies of the source room are indicated by dotted lines. The eigenfrequencies of the source room were predicted by means of a finite element model of the room, of which the results are shown in Fig. 14.

From Fig. 13 it can be seen that the acoustic pressure in the source room significantly peaks at the resonance frequencies of the source room when using the classical loudspeakers, whilst not when using the loudspeaker array. Also the response of the glazing is significantly higher at those resonance frequencies, in case of excitation by means of classical loudspeakers, which becomes evident from the higher sound powers radiated at those frequencies. In addition, the response of the glazing is also higher at its resonance frequencies (28 Hz, 62 Hz, 118 Hz), as expected. When using the loudspeaker array, the radiated sound power peaks at the first (28 Hz), second (62 Hz) and third (118 Hz) resonance frequencies of the glazing, as well as a peak at 41 Hz (see the black curves in Fig. 11 and Fig. 13b). Thus the loudspeaker array is capable to suppress the room modes in the source room, except for the room modes near 41 Hz.

Figure 7 shows the measured sound reduction index in $1/3^{\text{rd}}$-octave bands, according to the ISO standard. When processing the ISO microphone measurement data in narrow-bands, the results as shown in Fig. 15 are obtained. This result shows that the narrow band estimate of the sound reduction index significantly drops at the eigenfrequencies of the source room eigenmodes, whilst significantly increases at frequencies just below or just above the eigenfrequencies of the source room eigenmodes. The narrow band estimate of the sound reduction index based on measurements by means of the loudspeaker array does not show this dependency on the source room eigenmodes. These is however one exception. The narrow band estimate of the sound reduction index does show a dip around the room mode eigenfrequencies near 41 Hz (see Fig. 15b), in accordance with the observation discussed in the previous paragraph. This dip is not caused by a structural resonance frequency of the glazing (the first three eigenfrequencies of the glazing occurs near 28 Hz, 62 Hz and 118 Hz). This deficiency when using the loudspeaker array can be seen in all results presented in Fig. 10, Fig. 11 and Fig. 12. It shows the inability of the loudspeaker array to suppress the source room acoustics effect at this specific frequency.

The global trend of the narrow band sound reduction index R obtained by means of an array of loudspeakers and laser Doppler vibrometry corresponds well with the analytical model (ref Fig. 12 and the previous discussion in this section). The sound reduction index R obtained by means of an array of loudspeakers and laser Doppler vibrometry in terms of $1/3^{\text{rd}}$-octave frequency bands, however, shows significant deviations as compared to the measurements according to the ISO 10140-2:2010 standard for frequencies below 250 Hz, as shown in Fig. 7. The signature of both measurement results are the same, with dips at the 25 Hz and 62 Hz $1/3^{\text{rd}}$-octave fre-

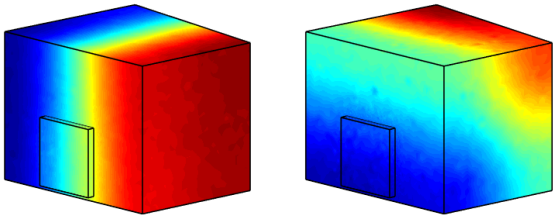

(a) mode 1, 34.15 Hz

(b) mode 2, 41.17 Hz

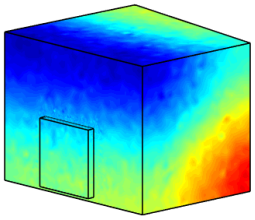

(c) mode 3, 41.61 Hz

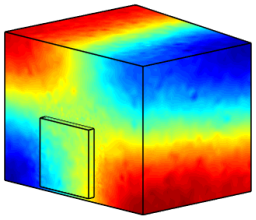

(d) mode 4, 53.94 Hz

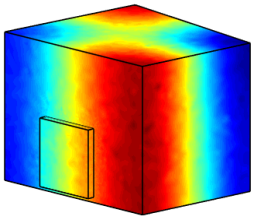

(e) mode 5, 54.18 Hz

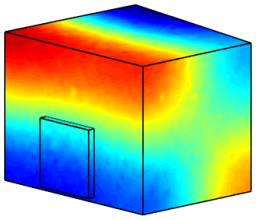

(f) mode 6, 58.49 Hz

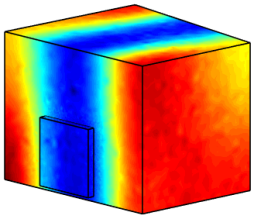

(g) mode 7, 67.07 Hz

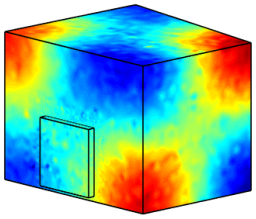

(h) mode 8, 68.42 Hz

Figure 14: Acoustic eigenmodes of the source room, as predicted by a finite element model of the source room. Test opening cove indicated by black lines.

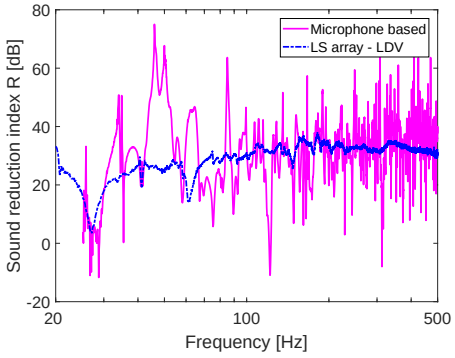

(a)

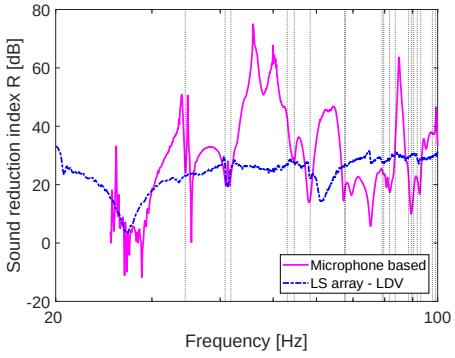

(b)

Figure 15: Narrowband sound reduction index R, using standardized microphone based approach (solid magenta curves) and using an array of loudspeakers and laser Doppler vibrometry (dashed blue curves). Top figure a) shows frequency range from 20 to 500 Hz, bottom figure b) shows frequency range from 20 to 100 Hz, acoustic resonance frequencies of source room indicated by vertical dotted black lines.

quency bands, corresponding to the structural resonance frequencies of 28 Hz and 62 Hz, respectively. However, deviations up to 15 dB are observed. This disagreement in the quantitative results of R in the lower frequency range is likely due to the room acoustic effects of the source room (volume 87 m^3), causing a breakdown of the diffuse field assumption. In the 250 Hz and 315 Hz $1/3^{rd}$-octave frequency bands the sound reduction index R obtained by means of an array of loudspeakers and laser Doppler vibrometry correspond well with the measurements according to the ISO 10140-2:2010 standard, with deviations of only 1 or 2 dB. At frequencies above 415 Hz, the loudspeaker array is not able to control the acoustic field because of insufficient spatial sampling, as discussed in Section 3.1.

3.3 Measurement effort in practice

In this section the actual measurement effort of the measurements on a single glazing, of lateral dimension 1.35×1.54 m^2, is summarized.

- The measurement of the matrix of transfer functions $\mathbf{H}$ between the acoustic responses $\mathbf{y}$ and the loudspeaker signals $\mathbf{x}$ with dimension $N_{mic} \times N_{LS} = 63 \times 12$, using a sweep excitation signal of 10 s with 3 averages took about 5 hours of measurement time, and an additional 5 hours for the manual positioning of the control microphone (63 positions), yielding a few GByte of time-domain data, using a sampling frequency of 4.41 kHz,

- The cross spectra of the structural responses $\mathbf{w}$ and the loudspeaker signals $\mathbf{x}$ with dimension $N_{LDV} \times N_{LS} = 266 \times 12$, whilst driving the loudspeaker array with the optimal signals $\mathbf{x}$, with a length of 10 s, 20 averages, 75 % overlap, took about 5 hours of measurement time, yielding about 11 GByte of time-domain data, using a sampling frequency of 4.41 kHz,

- The cross spectra of the acoustic responses $\mathbf{y}$ and the loudspeaker signals $\mathbf{x}$, with dimension $N_{mic} \times N_{LS} = 63 \times 12$, whilst driving the loudspeaker array with the optimal signals $\mathbf{x}$, with a length of 10 s, 20 averages, 75 % overlap, took about 1 hour of measurement time, and an additional 4 hours for the manual positioning of the control microphone (63 positions), yielding about 9 GByte of time-domain data, using a sampling frequency of 4.41 kHz.

In summary, the experiment took about 15 hours of measurement time (including manual positioning of the microphone), yielding about 20 GByte of data. Using multiple sensors, or a robot to replace the manually positioning of the sensor, would make the measurement easier to perform.

Note that it is required to have a record length which is at least equal to the reverberation time of the transmission facility [34], which forces the measurement time for each average to be about 10 seconds.

4 Conclusions

An array of loudspeakers was positioned closely to the building insulation element under test. The acoustic near field of the loudspeaker array was used to create a diffuse field, following the works of Bravo et al.. The method successfully suppressed the room acoustic modes of the source room for most of the frequencies below 150 Hz.

At the receiving side, the sound power radiated by the building element under test was computed from the measured vibration pattern of the building element. For this purpose the uncorrelated contributions to the total vibration pattern were determined using conditioned spectral analysis (CSA), followed by the application of the Rayleigh integral to compute the radiated sound power.

From the sound pressures measured at the surface of the building insulation element under test the incident sound power was determined. From the incident and radiated sound powers, the sound reduction index R was estimated. The estimation of the sound reduction index R of building elements by means of an array of loudspeakers and a scanning laser Doppler vibrometry was validated for a single glazing by means of an analytical model. The global trend corresponded well. In quantitative terms the narrow band results showed deviations up to 5 dB, which are probably due to the limited accuracy of the analytical model.

The newly proposed method is valid only in the lower frequency range due to the finite spatial sampling of the loudspeaker grid and structural response grid. For frequencies above the 200 Hz $1/3^{rd}$ octave band and up to the 630 $1/3^{rd}$ octave band the results obtained with the proposed method correspond to the standardized ISO 10140:2010 measurement results for the presented case, with deviations of only 1 or 2 dB's.

At frequencies below and including the 200 Hz $1/3^{rd}$ octave band large differences occurred up to 15 dB between the ISO measurements and both the analytical model and the newly proposed measurement approach. These deviations of the ISO results are likely to be caused by a breakdown of the diffuse field assumption.

As a side note it should be remarked that the loudspeaker array was not able to eliminate the room acoustic effects for all frequencies. This affected the sound reduction index estimate of the glazing at those specific frequencies (in the present case 41 Hz), causing a deviation of the narrow band measurement result as compared to the analytical solution result.

Although the method offers clear, strong points in terms of removing room acoustic effects from the measurements, a point of concern is the measurement effort. For a loudspeaker array consisting of 12 loudspeakers, the measurements of the blocking pressure at 63 microphone control positions, and the vibration response measurement at 266 positions with an averaging time of 60 sec per position, took tens of hours in total, yielding tens of GBytes of data. Moreover, a multichannel data acquisition is required, separate amplifiers for each loudspeaker of the array, and the construction of a (heavy) loudspeaker array cabinet.

Acknowledgments

This work was carried out in the framework of H2020-MSCA-RISE-2015 No. 690970 "Papabuild".

Willy Bruyninckx is acknowledged for performing the measurements according to the standard and Ludovic Labelle for his help in setting up part of the measurement equipment.

The research was conducted whilst the first author was working at KU Leuven. NBR is currently working at A&Z Acoustics, Bratislava.

A Evaluating the Rayleigh integral to compute the radiated sound power

Consider a vibrating baffled structure radiating into a semi-infinite acoustic domain. The structure is vibrating with a velocity field that is described by $v(\mathbf{x}_e, \omega)$. The parietal pressure at the points $\mathbf{x}_r$ on the structure can be computed by means of the Rayleigh integral [15, 36, 37]:

$$p\left(\mathbf{x}_r, \omega\right) = \frac{\mathrm{i}\omega\rho}{2\pi} \iint_S v_n\left(\mathbf{x}_e, \omega\right) \frac{e^{-\mathrm{i}kr}}{r} dS_r \tag{19}$$

where r is the distance between the points in vector $\mathbf{x}_e$ and vector $\mathbf{x}_r$, k is the wavenumber, ρ the density and ω the radial frequency. Note that the above integral has a singularity for $r \to 0$.

Equation 19 can be written in matrix form as

$$\mathbf{p} = \mathbf{Z}\mathbf{v} \tag{20}$$

where the matrix $\mathbf{Z}$ can be computed as follows [38], taking into account the singularity at $r \to 0$:

$$\mathbf{Z} = \rho c \begin{bmatrix} d & -\frac{ikS}{2\pi}\frac{e^{ikr_{ij}}}{r_{ij}} & \cdots \\ -\frac{ikS}{2\pi}\frac{e^{ikr_{ji}}}{r_{ji}} & d & \cdots \\ \vdots & \vdots & \ddots \end{bmatrix} \tag{21}$$

where

$$d = \frac{1}{2}\left(k\sqrt{\frac{S}{\pi}}\right)^2 - i\frac{8}{3\pi}\left(k\sqrt{\frac{S}{\pi}}\right) \tag{22}$$

Since the normal component of the active acoustic intensity I along the surface S of a vibrating test wall, is given by

$$I\left(\mathbf{x}_r, \omega\right) = \frac{1}{2}\mathrm{Re}\left[p\left(\mathbf{x}_r, \omega\right) v_n^*\left(\mathbf{x}_r, \omega\right)\right] \tag{23}$$

where Re denotes the real part of a complex quantity and the asterisk denotes the complex conjugate, the total radiated active sound power Π can be obtained by

$$\Pi\left(\omega\right) = \iint_S I\left(\mathbf{x}_r, \omega\right) dS \tag{24}$$

References

[1] ISO 717-1:2013, acoustics – rating of sound insulation in buildings and of building elements – part 1: Airborne sound insulation.

[2] ISO 16283-1:2014, acoustics – field measurement of sound insulation in buildings and of building elements – part 1: Airborne sound insulation.

[3] M. Rychtarikova, H. Muellner, V. Chmelik, N. B. Roozen, D. Urban, D. P. Garcia, C. Glorieux, Perceived Loudness of Neighbour Sounds Heard Through Heavy and Light-Weight Walls with Equal R-w + C50-5000, ACTA ACUSTICA UNITED WITH ACUSTICA 102 (1) (2016) 58–66.

[4] F. Ljunggren, C. Simmons, Airborne sound insulation between dwellings, from 50 Hz vs 100 Hz, a Swedish field survey, APPLIED ACOUSTICS 133 (2018) 58–63.

[5] ISO 10140-2:2010, acoustics – laboratory measurement of sound insulation of building elements – part 2: Measurement of airborne sound insulation.

[6] V. Hongisto, J. Keranen, M. Kylliainen, J. Mahn, Reproducibility of the Present and the Proposed Single-Number Quantities of Airborne Sound Insulation, ACTA ACUSTICA UNITED WITH ACUSTICA 98 (5) (2012) 811–819.

[7] C. Scrosati, F. Scamoni, M. Bassanino, M. Mussin, G. Zambon, Uncertainty analysis by a Round Robin Test of field measurements of sound insulation in buildings: Single numbers and low frequency bands evaluation - Airborne sound insulation, NOISE CONTROL ENGINEERING JOURNAL 61 (3) (2013) 291–306.

[8] M. Machimbarrena, C. R. A. Monteiro, S. Pedersoli, R. Johansson, S. Smith, Uncertainty determination of in situ airborne sound insulation measurements, APPLIED ACOUSTICS 89 (2015) 199–210.

[9] A. Tadeu, J. Antonio, D. Mateus, Sound insulation provided by single and double panel walls - a comparison of analytical solutions versus experimental results, Applied Acoustics 65 (1) (2004) 15 – 29.
URL http://www.sciencedirect.com/science/article/pii/S0003682X03001130

[10] C. Hopkins, P. Turner, Field measurement of airborne sound insulation between rooms with non-diffuse sound fields at low frequencies, APPLIED ACOUSTICS 66 (12) (2005) 1339–1382.

[11] E. d. A. C. Duarte, A. Moorhouse, E. B. Viveiros, Indirect measurement of acoustic power into a small room at low frequencies, APPLIED ACOUSTICS 73 (3) (2012) 248–255.

[12] T. Bravo, S. Elliott, Variability of low frequency sound transmission measurements, JOURNAL OF THE ACOUSTICAL SOCIETY OF AMERICA 115 (6) (2004) 2986–2997.

[13] J. Mahn, J. Pearse, The Uncertainty of the Proposed Single Number Ratings for Airborne Sound Insulation, BUILDING ACOUSTICS 19 (3) (2012) 145–172.

[14] T. Bravo, C. Maury, Enhancing low frequency sound transmission measurements using a synthesis method, JOURNAL OF THE ACOUSTICAL SOCIETY OF AMERICA 122 (2) (2007) 869–880.

[15] N. B. Roozen, L. Labelle, M. Rychtarikova, C. Glorieux, Determining radiated sound power of building structures by means of laser Doppler vibrometry, JOURNAL OF SOUND AND VIBRATION 346 (2015) 81–99.

[16] S. Elliott, C. Maury, P. Gardonio, The synthesis of spatially correlated random pressure fields, JOURNAL OF THE ACOUSTICAL SOCIETY OF AMERICA 117 (3, 1) (2005) 1186–1201.

[17] T. Bravo, C. Maury, The experimental synthesis of random pressure fields: Methodology, JOURNAL OF THE ACOUSTICAL SOCIETY OF AMERICA 120 (5, 1) (2006) 2702–2711.

[18] C. Maury, T. Bravo, The experimental synthesis of random pressure fields: Practical feasibility, JOURNAL OF THE ACOUSTICAL SOCIETY OF AMERICA 120 (5, 1) (2006) 2712–2723.

[19] A. Piersol, Use of coherence and phase data between 2 receivers in evaluation of noise environments, JOURNAL OF SOUND AND VIBRATION 56 (2) (1978) 215–228.

[20] H. Nelisse, J. Nicolas, Characterization of a diffuse field in a reverberant room, JOURNAL OF THE ACOUSTICAL SOCIETY OF AMERICA 101 (6) (1997) 3517–3524.

[21] F. Jacobsen, T. Roisin, The coherence of reverberant sound fields, JOURNAL OF THE ACOUSTICAL SOCIETY OF AMERICA 108 (1) (2000) 204–210.

[22] M. N. Ichchou, B. Hiverniau, B. Troclet, Equivalent 'rain on the roof' loads for random spatially correlated excitations in the mid-high frequency range, JOURNAL OF SOUND AND VIBRATION 322 (4-5) (2009) 926–940.

[23] C. Marchetto, L. Maxit, O. Robin, A. Berry, Vibroacoustic response of panels under diffuse acoustic field excitation from sensitivity functions and reciprocity principles, JOURNAL OF THE ACOUSTICAL SOCIETY OF AMERICA 141 (6) (2017) 4508–4521.

[24] J. Bendat, A. Piersol, Engineering applications of correlation and spectral analysis., Wiley-Interscience, NewYork, 1980.

[25] S. M. Price, B. R. J., Virtual coherence: a digital signal processing technique for incoherent source identification, in: Proceedings of IMAC 4, 1986.

[26] Q. Leclere, Multi-channel spectral analysis of multi-pass acquisition measurements, MECHANICAL SYSTEMS AND SIGNAL PROCESSING 23 (5) (2009) 1415–1422.

[27] G. Shu, X. Liang, Identification of complex diesel engine noise sources based on coherent power spectrum analysis, MECHANICAL SYSTEMS AND SIGNAL PROCESSING 21 (1) (2007) 405–416.

[28] M. H. Fouladi, M. J. M. Nor, A. K. Ariffin, Spectral analysis methods for vehicle interior vibro-acoustics identification, MECHANICAL SYSTEMS AND SIGNAL PROCESSING 23 (2) (2009) 489–500.

[29] R. Waterhouse, Interference patterns in reverberant sound fields, JOURNAL OF THE ACOUSTICAL SOCIETY OF AMERICA 27 (2) (1955) 247–258.

[30] F. Jacobsen, The diffuse sound field, Tech. rep., Note no 27, Technical University of Denmark (1979).

[31] P. Gardonio, M.J. Brennan, Mobility and impedance methods in structural dynamics, in: F. Fahy, J. Walker (Eds.), Advanced Applications in Acoustics, Noise and Vibration, London, 2004, pp. 389-447.

[32] A. J. Jerri, The shannon sampling theorem - its various extensions and applications - a tutorial review, Proceedings of the IEEE 65 (11) (1977) 1565–1596.
URL <GotoISI>://WOS:A1977EB77800004

[33] V. Wittstock, On the uncertainty of single-number quantities for rating airborne sound insulation, ACTA ACUSTICA UNITED WITH ACUSTICA 93 (3) (2007) 375–386.

[34] N. B. Roozen, Q. Leclere, M. Rychtarikova, C. Glorieux, A global error estimator for the uncertainty of a multi-channel spectral analysis, APPLIED ACOUSTICS 87 (2015) 57–63.

[35] N. B. Roozen, Q. Leclère, D. Urbán, T. M. Echenagucia, P. Block, M. Rychtáriková, C. Glorieux, A hybrid experimental numerical approach to assess the airborne sound insulation from mobility measurements, JOURNAL OF SOUND AND VIBRATION, 2018.

[36] G. Koopmann, H. Benner, Method for computing the sound power of machines based on the Helmholtz integral, JOURNAL OF THE ACOUSTICAL SOCIETY OF AMERICA 71 (1) (1982) 78–89.

[37] F. Fahy, Sound and Structural Vibration: Radiation, Transmission and Response., Academic Press, London, 1985.

[38] M. Bai, M. Tsao, Estimation of sound power of baffled planar sources using radiation matrices, JOURNAL OF THE ACOUSTICAL SOCIETY OF AMERICA 112 (3, 1) (2002) 876–883.